ACS APPLIED ENERGY MATERIALS

Article

Charge carrier transport, trapping, and recombination in PEDOT:PSS/n-Si solar cells

Serhiy Kondratenko, Volodymyr Lysenko, Yury V. Gomeniuk, Olga Kondratenko, Yury Kozyrev, Oleksandr Selyshchev, Volodymyr Dzhagan, and Dietrich R. T. Zahn

ACS Appl. Energy Mater., **Just Accepted Manuscript** • DOI: 10.1021/acsaem.9b01083 • Publication Date (Web): 29 Jul 2019

Charge carrier transport, trapping, and recombination in PEDOT:PSS/n-Si solar cells

Serhiy Kondratenko[†],* Volodymyr Lysenko,[‡] Yury V. Gomeniuk,[‡] Olga Kondratenko,[‡] Yury Kozyrev,[§] Oleksandr Selyshchev,[‖] Volodymyr Dzhagan,[†,‡] Dietrich R.T. Zahn, [‖]

[†] Taras Shevchenko National University of Kyiv, 64 Volodymyrs'ka St., 01601, Kyiv, Ukraine

[‡] V. E. Lashkaryov Institute of Semiconductors Physics, NAS of Ukraine, 41 pr. Nauki, 03028, Kyiv, Ukraine

[§]O.O. Chuiko Institute of Surface Chemistry, 17 Generala Naumova St., 03164, Kyiv, Ukraine

[‖] Semiconductor Physics, Chemnitz University of Technology, D-09107 Chemnitz, Germany

Abstract

The effect of interface states on electrical transport mechanisms in PEDOT:PSS/n-Si solar cells (SCs) was investigated using admittance spectroscopy, current-voltage (J-V) and capacitance-voltage (C-V) measurements. The J-V dependences measured in the temperature range of 80 - 300 K can be described by an equivalent circuit for a two-diode model including parallel and serial resistances. From the analysis of the temperature dependence of the J-V curves, the role of the silicon oxide layer in charge carrier transport in the hybrid solar cell (SC) was clarified. A density of states of 2.5×10^{10} $cm^{-2}eV^{-1}$ localized at the SiO_2/Si interface at E_v+0.3 eV is deduced from admittance measurements. The low density of electrically active defects near the Fermi level and an interface recombination rate of 480 cm/s indicate a good passivation of the

PEDOT:PSS/nSi interface. The interfacial defects associated with dangling bonds (P_b centers) at the polymer-silicon interface are responsible for an increase of the series resistances and the dominance of the recombination current at forward biases.

Keywords: organic-inorganic heterojunction, admittance spectroscopy, interface traps, recombination, solar cells.

1. Introduction

Poly(3,4-ethylenedioxythiophene) blended with poly(4-styrenesulfonic acid) (PEDOT:PSS) is a heavily doped p-type organic semiconductor with a bandgap of around 1.6 eV,[1] which shows currently great promise as transparent electrode material for various applications in organic electronics and next generation photovoltaics because of its high conductivity and transmission window in the visible range.[2,3]

Recently, considerable progress in producing highly efficient organic-inorganic solar cells (SCs) by spin-coating of aqueous PEDOT:PSS solutions on n-type silicon (n-Si) surfaces with subsequent annealing was reported by many groups.[4-6] Contrary to the complex technology required for the production of silicon solar cells, the organic-silicon heterojunctions have some advantages including low-temperature, vacuum-free, and therefore low-cost fabrication processes. A power conversion efficiency (PCE) of over 14% for junctions without antireflection coating is the consequence of the formation of a potential barrier of 0.7 eV at the organic-inorganic interface.[4] Its height is determined mainly by the difference between the work functions of the top Au contact and n-Si. To enhance the performance of planar PEDOT:PSS/n-Si SCs, different approaches including Si surface passivation by SiO_x,[7] methyl/allyl monolayers,[8]

adding of a co-solvent,[9,10] graphene oxide,[11] formation of silicon nanowire arrays,[12] as well as optimization of the rear contact between Si and the metal electrode were proposed.[13]

The electrical output of hybrid devices critically depends on the properties of the interface between Si and PEDOT:PSS. A low density of states is highly important for achieving a strong inversion near the silicon surface because devices with a large defect density typically form a depletion layer. In turn, the nature of interface traps is greatly affected by the type of the surfactant used to increase the wettability of PEDOT:PSS on H-terminated silicon surfaces, thickness and continuity of polymer films, thickness of the native SiO_x layer, annealing temperature, and sample storage conditions after the spin-coating process. Understanding the influence of all these factors helps to optimize the performance of photovoltaic devices and reach high efficiencies close to the Shockley–Queisser limit.[14]

Despite much effort to describe the charge transport in PEDOT:PSS/n-Si there is no good understanding of the formation of interface states and their effect on the device performance.[15-18] A simplified approach assumes that the PEDOT:PSS/n-Si structure is a Schottky junction, where the organic polymer acts as a metallic electrode.[6]However, such a description is not sufficient to explain the electron transport of hybrid SCs. The main reason is that the lowest unoccupied molecular orbital (LUMO) band of PEDOT is much higher than the conduction band of Si. As a result, the thermionic emission of electrons from Si into PEDOT is blocked. If we assume that the highest occupied molecular orbital (HOMO) band is aligned with the valence band of Si, an extra current associated with recombination at the interface between PEDOT:PSS and n-Si should be observed. Thereby, the transport properties of the studied heterojunction can be predicted when the conduction band offset, the nature of interface defects, as well as rate of recombination via interface states are taken into account.

In the present study the electrical properties of PEDOT:PSS/n-Si heterojunctions were studied in detail by dark current density-voltage and small signal capacitance-voltage measurements as well as admittance spectroscopy technique. The J-V curves at different temperatures were analyzed in the framework of a two-diode model to extract the energies of the interface traps and to determine the mechanisms of charge carrier transport.

2. Experimental details

Double-side-polished n-type Si(100) phosphorus-doped wafers with a resistivity of 4.5 Ω·cm and thickness of 500 μm were used as a substrate. The Si samples (1.2 x 1.2 cm^2) were cleaned by ultrasonicationin acetone, ethanol, and deionized water for 20 min each at 30°C. Subsequently they were dipped in 30% hydrofluoric (HF) acid to remove the native silicon oxide layer. In order to increase the conductivity and ensure a proper surface uniformity of the polymer film, 5% vol% dimethyl sulfoxide (DMSO) as a secondary dopant and surfactant (0.025 vol% sodium dodecyl sulfate) were added to the PEDOT:PSS solution. The water based solution was filtered with a polyvinylidene fluoride membrane (0.45 μm porosity) to remove agglomerations. Then, the PEDOT:PSS solution was spin coated at 3000 rpm for 20 s followed by thermal annealing at 140°C for 30 min under standard atmospheric conditions.

Small area diodes (0.05–0.06 cm^2) with continuous Au electrode were produced for capacitance-voltage (C-V), dark current-voltage (J-V), and admittance measurements in order to avoid uncertainties with interpretation when considering an equivalent circuit model. Reference junctions, *i.e.* Au/SiO_2/n-Si and Au/PEDOT:PSS/SiO_2/n-Si with 2.4 nm native silicon oxide films, were also produced. To evaluate photovoltaic properties, a gold grid pattern with a finger width of 180 μm, and inter-finger spacing of 330 μm was evaporated thermally through a

shadow mask on the PEDOT:PSS surface (1.2 x 1.2 cm^2). An In/Ga eutectic was scratched into the silicon substrate as a back contact.

The upper inset in Figure 1a shows a schematic of the Au/PEDOT:PSS/nSi solar cells. The short circuit current density J_{sc} was essentially constant at around ~20.5 mA/cm^2 and the open-circuit voltage around ~0.56 V measured under AM1.5G and a light intensity of 100 mW/cm^2 (Figure S2). The fill factor (FF) for the J-V curves was in the range from 55% to 60% for different samples prepared in the same conditions. The produced hybrid solar cells show efficiencies around 7%, while the gold electrode resulted in a high optical loss of 35% of the incident light intensity due to shadowing.

The PEDOT:PSS surface topology as well as the roughness were controlled using atomic force microscopy (AFM) before gold deposition. The AFM measurements were performed with an NT-MDT Ntegra microscope in semi-contact tapping mode using Si cantilevers with a tip apex radius of about 10 nm. A surface roughness (rms) of 1.8 nm is found from AFM image analysis of PEDOT:PSS surface (see Figure S1 in the Supporting Information).

The junctions were characterized by capacitance-voltage (C-V), conductance vs. frequency (G-ω), and J-V measurements in a temperature range between 80 – 300 K using an Agilent 4284A LCR meter, Agilent B1500A, and Agilent 4156C Semiconductor Parameter Analyzers, respectively.

The optical constants and thicknesses of the PEDOT:PSS and silicon oxide films were studied using spectroscopic ellipsometry. The ellipsometry characterization of those parts of the samples uncovered with Au was performed using a SE-2000 SEMILAB ellipsometer which spans the NIR–VIS–UV range (190–2000 nm) with a resolution of 5 nm. The measured spectral dependences of the amplitude component ψ (a) and phase difference Δ (b) of the

PEDOT:PSS/n-Si heterostructure are presented in Figure S3 (see Supporting Information). A four layer model comprising the Si(001) substrate, interfacial (oxide) layer, PEDOT:PSS thin film, and a surface roughness layer was used for fitting the experimental data. The PEDOT:PSS film thickness, the interfacial layer thickness, and the optical constants of PEDOT:PSS films were obtained simultaneously by standard ellipsometric data fitting procedures involving Drude and Cauchy models for the PEDOT:PSS layer, as well as the known dielectric function of the Si substrate and the native silicon dioxide. The thickness of the polymer layer on Si(001) and SiO_2/Si(001) wafers was found to be around (45±1) nm and (47±1) nm, respectively. The thickness of native silicon dioxide was found to be (2.4±0.1) nm and (2.5±0.1) for the SiO_2/Si(001) wafer before and after covering by polymer film, respectively, while the interfacial layer between PEDOT:PSS and HF-etched silicon substrate was thinner (1.6±0.1) nm.

X-ray Photoelectron Spectroscopy (XPS) and Ultraviolet Photoelectron Spectroscopy (UPS) studies were performed using an ESCALAB™ 250Xi Microprobe (Thermo Scientific) spectrometer, equipped with 1486.6 eV monochromatic Al Kα X-ray source, and 21.2 eV He I line UV-source, respectively. XPS spectra were measured with an analyzer pass energy of 20 eV (resolution 0.6 eV). UPS spectra were taken with a pass energy of 1.0 eV (0.1 eV).

3. Results

3.1. Current-voltage and capacitance voltage measurements. In order to describe the performance of hybrid organic-silicon SCs and highlight the role of PEDOT:PSS thin films, we measured the electrical characteristics of PEDOT:PSS/n-Si heterojunction. Figure 1a shows the representative $J-V$ characteristics for Au/PEDOT:PSS/n-Si heterojunction measured under dark conditions at different temperatures. As can be seen, a strong rectification with the current at reverse bias being an order of magnitude lower than that at forward bias indicates that a high

potential barrier exists near the PEDOT:PSS/n-Si interface. The forward (reverse) regime is obtained for a positive (negative) voltage applied to Au top electrode. The rectifying behavior which increases with decreasing temperature was also observed for the Au/SiO_2/n-Si reference structures and for the hybrid Au/PEDOT:PSS/SiO_2/n-Si junctions with the PEDOT:PSS solution spin-coated on the native silicon oxide surface (Figure 1b).

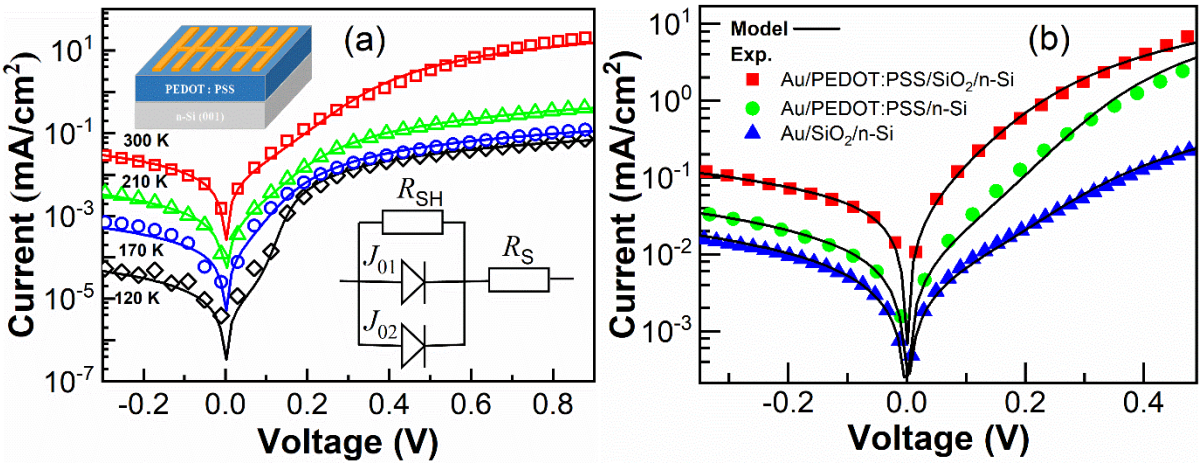

Figure 1. (a) $J-V$ characteristics for a Au/PEDOT:PSS/n-Si sample measured under dark conditions at different temperatures. The insets are a schematic of the Au/PEDOT:PSS/n-Si diode and equivalent scheme of the studied junctions. (b) $J-V$ characteristics for Au/PEDOT:PSS/n-Si, Au/SiO_2/n-Si, and Au/PEDOT:PSS/SiO_2/n-Si junctions measured under dark conditions at 300 K. The points represent the measured data and lines are the best fit to the data with the two-diode model based on J_{01}, J_{02}, serial and shunt resistances as parameters.

The shape of the curves was analyzed within the framework of the two-diode model assuming bulk diffusion and recombination process via traps in the space-charge region taking into account the impact of serial and shunt resistance.[19] Here the current density, *J*, is given by:

$$J(V) = J_{01}\left(\exp\left(\frac{e(V-JR_S)}{kT}\right)-1\right)+J_{02}\left(\exp\left(\frac{e(V-JR_S)}{2kT}\right)-1\right)+\frac{V-JR_S}{R_{SH}}, \quad (1)$$

where k is the Boltzmann's constant, T is the absolute temperature, R_S and R_{SH} are the series and shunt resistances, J_{01} is saturation current density corresponding to bulk diffusion, while J_{02}

represents recombination process via traps in the space-charge region. The 2/3-Diode software [20] was used to fit the experimental J-V curves measured in the temperature range from 120 K to 300 K with a step of 10 K. As a result, a set of fitting parameters of J_{01}, J_{02}, R_S and R_{SH} was determined for a given J-V curve allowing to determine their temperature dependences.

To clarify the charge transport mechanism in PEDOT:PSS-n-Si the temperature dependence of the saturation current was analyzed. At forward bias, the direct current is limited by two physical processes: (i) the thermionic emission of electrons from n-Si over the energy barrier, and (ii) injection of holes from PEDOT:PSS into the space-charge region of Si. The first one is a Schottky effect leading to a temperature dependence of the saturation current for a diode as:

$$J_{01} = A^* T^2 \exp\left(-\frac{\phi_B}{kT}\right), \quad (2)$$

where A* is the effective Richardson constant, T is the temperature, k is the Boltzmann constant, and ϕ_B is the barrier height. With decreasing temperature, the probability of this mechanism decreases proportionally to $\exp\left(-\frac{\phi_B}{kT}\right)$, whereby the electron transport component of the current cannot be distinguished at temperatures below 265 K from the background of the dominating recombination current, which is described by the second term of Eq.(1). As a consequence, the value of J_{01} was extracted from J-V curves measured in the narrow temperature range from 265 K to 295 K. Figure 2a presents the temperature dependence of the saturation current density, J_{01}. The barrier height of ϕ_B = (740±10) meV and ϕ_B = (330±10) meV were estimated from the slope of the $\ln\left(J_{01}/T^2\right)$ vs $1/kT$ Arrhenius plot of the Au/PEDOT:PSS/n-Si and Au/SiO_2/n-Si junctions, respectively. In comparison with organic-silicon junction, an order of magnitude higher value of J_{01} and twice lower potential barrier is

observed for the Au/SiO_2/n-Si reference Schottky diode (see Fig.2a). The potential barrier heights derived from J-V data are in good agreement with C-V measurements, which are described below.

The dominance of the recombination conduction mechanism at forward bias was observed for the all diodes in the studied temperature range. In contradistinction to the classical Schottky junction, when the forward current is due to majority carrier injection from n-Si to the Au electrode, the PEDOT:PSS effectively limits the electron injection into its LUMO band due to the conduction band offset of around 0.45 eV to Si.[4] As a consequence, the most likely way for electrons to contribute to the forward current is recombination with holes in the space-charge region of Si or/and via PEDOT:PSS/n-Si interface traps. Figure 2b presents the temperature dependence of saturation current J_{02} in the range from 120 K to 295 K for sample with PEDOT:PSS on Si surface. The activation energies (290±10) meV and (130±10) meV were determined from the approximation of two linear parts of the Arrhenius plot $\ln(J_{02})$ vs $1/kT$. For holes in the PEDOT:PSS film, the injection to the space-charge region of n-Si involves overcoming a potential barrier the height of which is determined by the energy distance between the Fermi level and the top of the valence band of the Si substrate. The derived activation energy of (290±10) meV is close to the valence band offset reported for PEDOT:PSS/Si junctions.[4] At low temperatures, when thermionic emission becomes less probable, hole trap levels with energy of (130±10) meV are responsible for the recombination current through PEDOT:PSS/n-Si interface. In comparison with hybrid junctions, the Au/SiO_2/n-Si Schottky diodes show a lower value of J_{02} due to the presence of a native oxide layer SiO_2, which limits the current. Its temperature dependence is determined by the presence of electron traps near SiO_2/n-Si interface,

the energies of which $E_{C,1}$-(100±10) meV and $E_{C,2}$-(220±10) meV were extracted from the slopes of linear parts of the $\ln(J_{02})$ vs $1/kT$ dependence (Fig.2b).

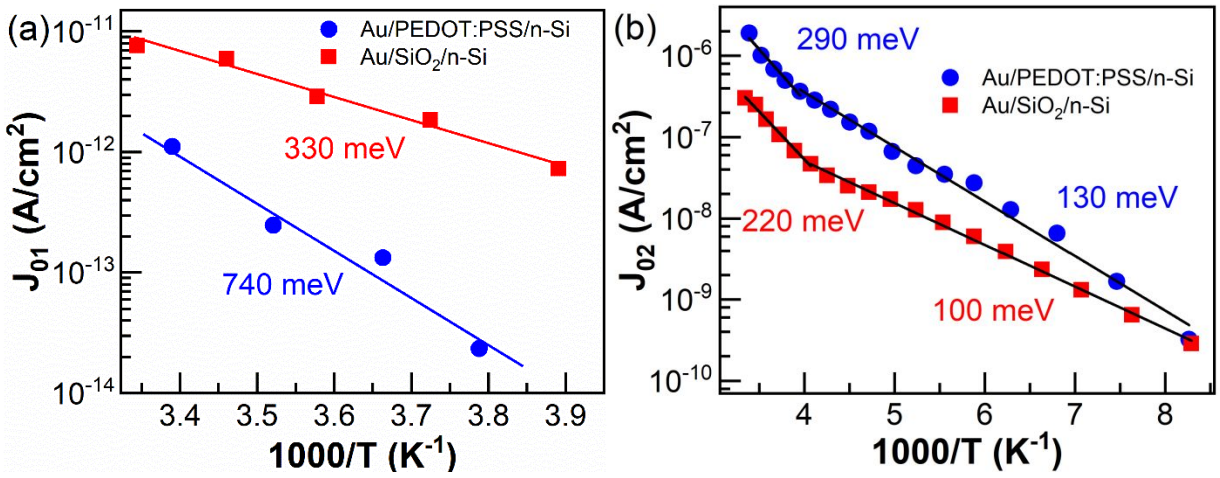

Figure 2. (a) Arrhenius plots showing the calculated barrier height (740±10) meV and (330±10) meV for Au/PEDOT:PSS/n-Si and Au/SiO_2/n-Si diodes, respectively; (b) temperature dependences of J_{02} for Au/PEDOT:PSS/n-Si (●) and Au/SiO_2/n-Si (■).

To clarify the impact of interface traps on charge transport in organic-silicon junctions it is important to analyze their effect on series and parallel resistances. Figure 3a shows the temperature dependence of the serial resistance of the Au/PEDOT:PSS/n-Si diode, where three different regions can be distinguished. At temperatures T> 210 K (region I), the R_S decreases with increasing temperature indicating the thermal activation of holes. In this region, $R_S(T)$ can be represented as:

$$R_S(T) = R_{S0}\exp\left(-\frac{E_A}{kT}\right), \quad (3)$$

where R_{S0} is an exponential prefactor, E_A is the activation energy. A similar behavior was observed for the temperature range from 170 to 210 K (region II). The linear parts of $\ln R_S(T)$ vs $1/kT$ plot are fitted and extrapolated to extract from the slopes the activation energies of (270±10) meV and (100±10) meV for the regions I and II, respectively. At low temperatures

(120-170 K, region III), the dependence of the serial resistance on temperature was found to be weak and did not show an Arrhenius behavior. It should be noted that the derived activation energies were found to be close to the values obtained from the analysis of $J_{02}(T)$. We can conclude that the temperature dependence of the serial resistance and the recombination current are determined by the same traps localized at the interface layer between PEDOT:PSS and silicon. Their appearance is due to the fact that a thin layer of SiO_x is formed after the Si substrate is taken out from the HF solution. Zhang *et al.*[7] reported about the formation of a silicon oxide layer with a thickness of 0.87 nm for SiO_x layer immediately after the HF etching process. During short (less than 20 s) exposition to air, oxygen tends to react with Si by replacing H-terminated bonds that can enhance wettability required for the production of continuous PEDOT:PSS films. From one point of view, SiO_x suppresses the recombination velocity due to the separation of charge carriers by an internal electric field at the interface.[21] However, the thin oxide layer increases the interfacial electrical resistance that limits the forward current and deteriorates the transport properties of the hybrid solar cell.

A thicker (2.5 nm) silicon oxide layer in the Au/SiO_2/n-Si diode also leads to the observation of a higher series resistance because of its electrically insulating nature. We analyzed the temperature dependence of serial and shunt resistances of the Au/SiO_2/n-Si diodes. As shown in Figure 3a, the serial resistance was much higher in the high-temperature range in comparison with the organic-silicon diode. An Arrhenius plot of $\ln R_S(T)$ vs $1/kT$ provides the activation energy of (100±5) meV. Note that this activation energy coincides with the value derived for Au/PEDOT:PSS/n-Si diode in the 170-210 K range. We can conclude that the serial resistance in this temperature range is determined by the properties of the interfacial oxide layer. At the same time, at higher temperatures, T>210 K, the forward current is limited by the efficiency of hole

emission from PEDOT:PSS to Si, the probability of which increases with the valence band offset ΔE_v. The estimate of (270±10) meV, derived from the analysis of $R_S(T)$ in 210-300 K range, is in a good agreement with values determined from the linear part of $\ln(J_{02})$ vs $1/kT$ plot.

The shunt resistance of the Au/PEDOT:PSS/n-Si diode varies from 10.2 kΩ·cm^2 at 295 K to 6.6 MΩ·cm^2 at 120 K (Fig.3b). From the Arrhenius plot of $\ln R_{SH}(T)$ vs $1/kT$, the activation energies of (100±10) meV and (160±10) meV were determined. The leakage current, which gives a significant contribution at reverse biases, originates from a number of microvoids in the PEDOT:PSS film, which are usually formed during the spin-coating process on Si substrates with poor wettability.[10] Further thermal evaporation of the Au electrode on top of the discontinuous polymer film results in the appearance of local Au/SiO_x/n-Si Schottky microjunctions. These regions differ in electron transport properties from the silicon surface covered by the polymer with hole-selective nature. Being the majority carriers in silicon, electrons contribute predominantly to conductivity via the local voids without blocking by PEDOT:PSS. This process is facilitated by defects of both the Au/SiO_x and Au/Si interfaces, which causes a local lowering of the potential barrier as compared to regions with PEDOT:PSS. It enhances charge carrier recombination and therefore increases the leakage current.[19] For the Au/SiO_2/n-Si diodes, the shunt resistance was much lower than that observed for organic-silicon junctions at T<210 K, while R_{SH} becomes independent of temperature. The possible reason of the strong leakage is a high density of defects at the silicon oxide surface covered with Au.

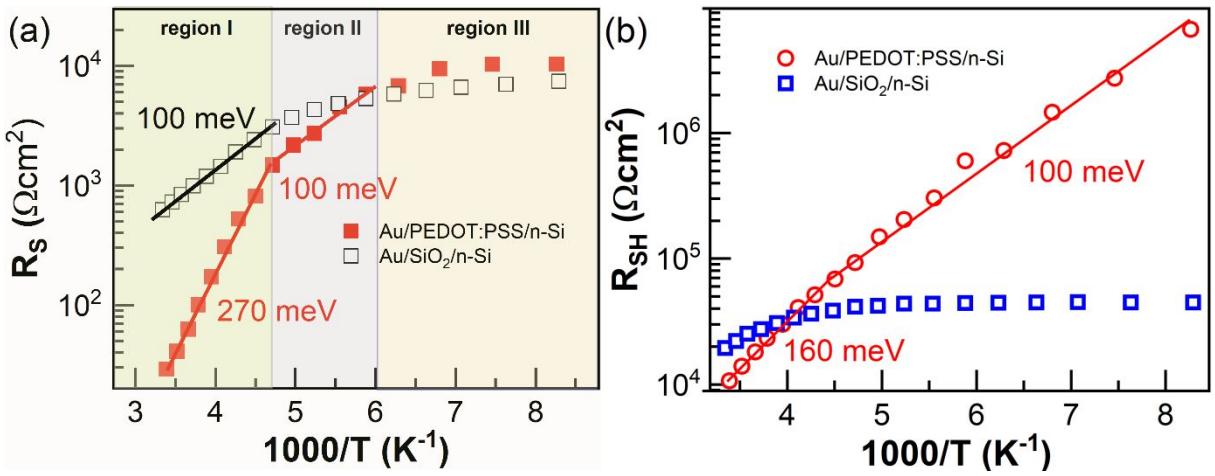

Figure 3. Temperature dependences of serial (a) and shunt (b) resistances of the Au/PEDOT:PSS/n-Si and Au/SiO_2/n-Si diodes.

3.2. Capacitance voltage measurements and admittance spectroscopy. Figure 4 shows experimental capacitance-voltage (C-V) characteristics of the Au/PEDOT:PSS/n-Si (curve 1), Au/SiO_2/n-Si (curve 2), and Au/PEDOT:PSS/SiO_2/n-Si diode (curve 3) measured at a modulation frequency of 1 MHz and temperature of 295 K. The depletion layer capacitance of the diodes at reverse bias can be described as follows

$$\frac{1}{C_b^2} = \frac{2\left(V_{bi} - V - \frac{kT}{q}\right)}{q\varepsilon_0\varepsilon_s A^2 N_D}, \qquad (3)$$

where V_{bi} is the built-in potential; A the diode area; $\varepsilon_0\varepsilon_s$ the permittivity of silicon; N_D the dopant concentration of silicon; k the Boltzmann constant; T the temperature; V the applied voltage; q the elementary charge. A built-in potential of $\phi_B = qV_{bi}$ = (615±5) meV for the hybrid junctions (curves 1 and 3) was extracted from the V-axis intercepts. A lower potential barrier of (300±5) meV is observed for the inorganic Au-SiO_2-n-Si diodes due to Fermi level pinning at the defects of the SiO_2/Si interface and Au-induced surface states, which is usually observed at Schottky junctions with silicon.

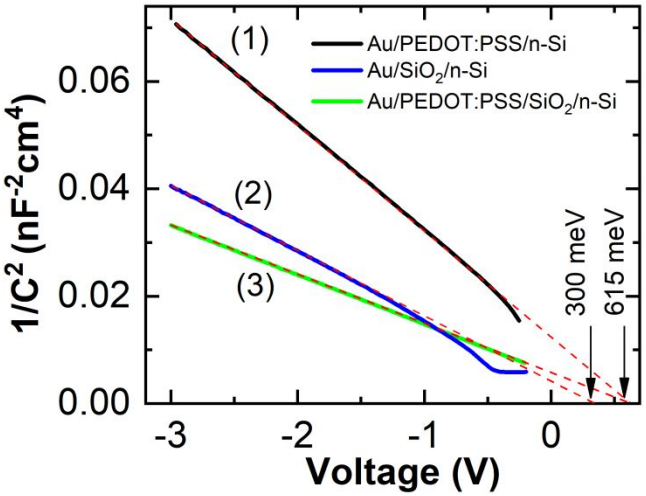

Figure 4. TheC-V characteristics of the Au/PEDOT:PSS/n-Si (curve 1), Au/SiO_2/n-Si (curve 2) and Au/PEDOT:PSS/SiO_2/n-Si diode (curve 3) measured at a modulation frequency of 1 MHz and temperature of 295 K.

Admittance spectroscopy [22] (measurement of ac conductance G and capacitance C as a function of temperature T and frequency f) was proven in its effectiveness to extract defect parameters in *p-n* junctions,[23,24] heterostructures,[25] Schottky diodes [26] and MIS-capacitors [27]. The $G(T)/\omega$ curves for a given measurement frequency $\omega=2\pi f$ exhibit a maximum at T_{max} which depends on the activation energy and the capture cross section of a trap, while the amplitude is proportional to the number of electrons contributing to the charging/discharging process. In most cases the conductance peak is attributed to recharging of deep traps inside the semiconductor bulk, but if interface electronic states are present at the heterointerface or metal-semiconductor interface then they also may contribute to the ac response.[28,29]

The conductance spectra of the Au/PEDOT:PSS/n-Si and Au/SiO_2/n-Si junctions measured at different frequencies are shown in Figure 5 (a) and (b), respectively. Peaks in the spectra of the Au/SiO_2/n-Si junction were taken at much higher modulation frequencies than for the Au/PEDOT:PSS/n-Si junction. If we suggest that the peak value of G/ω is related to the bulk

density of deep states in the semiconductor, then this density value should be the same for both samples, since we used the same *n*-type silicon wafer for sample preparation. To check this, we performed the analysis of $C(\omega)$ dependences following the approach of Ref. [30], where the trap density of states is calculated from the derivative of the capacitance with respect to the frequency. Calculations, however, yielded magnitudes of the trap density which differ by a factor of 3 for the two samples. Therefore, it is reasonable to relate the peak value of G/ω to the density of interface states at the silicon/dielectric interface and not to the trap density of states in the bulk. In this case the density of interface states, D_{it}, is given by the equation $D_{it}=2.5G/(\omega \cdot q \cdot A)$, where q is the electron charge and A is the sample area.[31] The interface states densities of traps responsible for the detected admittance peak at the given frequency are equal to 2.5×10^{10} $cm^{-2}eV^{-1}$ and 3.0×10^{10} $cm^{-2}eV^{-1}$ for Au/PEDOT:PSS/n-Si and Au/SiO_2/nSi structures, respectively. From Arrhenius plots of $\ln(T_{max}^2/\omega)$ (see insets in Figure 5a,b) activation energies of $E_a = (0.31\pm0.01)$ eV and (0.25 ± 0.01) eV were derived for the Au/PEDOT:PSS/nSi and Au/SiO_2/n-Si structures, respectively. These values are close to the depth of P_b traps[32], which are related to dangling bond states at the SiO_2/Si interface with two peaks of D_{it} at E_v+0.3 eV and E_v+0.8 eV. The presence of such centers in the Au/PEDOT:PSS/n-Si sample can be explained by the appearance of a thin interfacial SiO_x layer between PEDOT:PSS and silicon due to native oxidation of silicon during the SC production. P_b centers were also detected in samples with high-k dielectric (Gd_2O_3 and Nd_2O_3) layers on silicon.[33] As for the Au/PEDOT:PSS/n-Si junction, the determined activation energy of 0.31 eV corresponds to the contribution of E_v+0.3 eV hole traps to the admittance signal, nearest to the Fermi level, which leads to the observation of the G/ω peak at low modulation frequencies. By contrast, the majority carriers, electrons in nSi, contribute mainly to the admittance response of the Au/SiO_2/n-Si Schottky junction. The

states of P_b centers close to the peak at E_c-0.25 eV (or E_v+0.8 eV) are responsible for a faster electron exchange and therefore the observation of the admittance signal at higher modulation frequencies as compared to the Au/PEDOT:PSS/nSi diode.

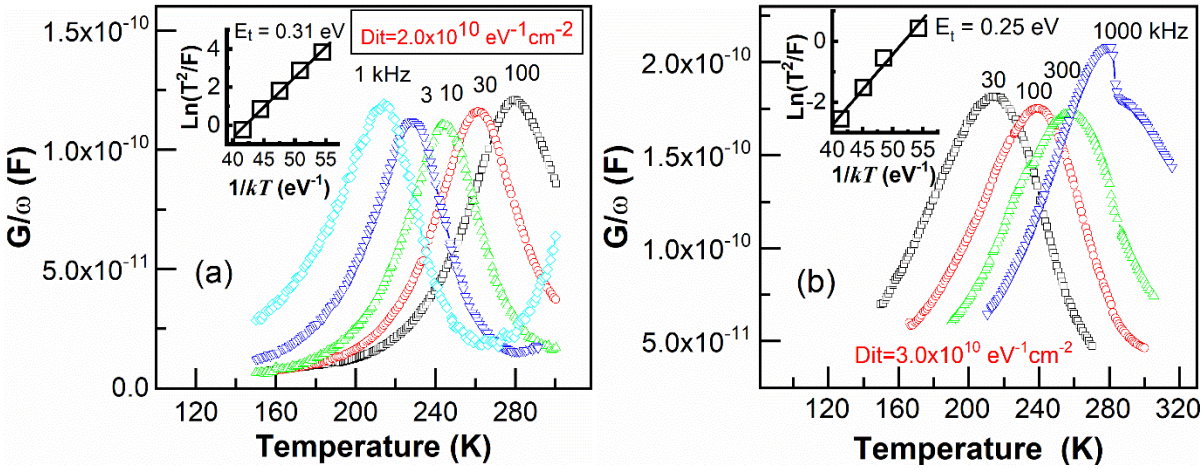

Figure 5. Conductance spectra of the Au/PEDOT:PSS/n-Si sample (a) and Au/Sio$_2$/n-Si sample (b) measured with different modulation frequencies. Insets show the respective Arrhenius plots of $\ln(T_{max}^2/\omega)$ obtained from the $G(T)/\omega$ curves.

Another fact that should be mentioned is the different width of the admittance peaks for the junctions with and without PEDOT:PSS. One can see in Fig. 5, that in the Au/PEDOT:PSS/n-Si sample the peaks are more narrow. The full width at half maximum equals to 36 K for the sample with PEDOT:PSS layer and 56 K for the control Au/SiO_2/n-Si Schottky diode. This difference is due to different potential fluctuations at the silicon surface for the two samples. Taking into account the shift of the Fermi level with temperature, the widening of the peaks along the temperature scale can be converted into a variation of the Fermi potential at the surface. The potential fluctuations at the interface $\Delta\psi_s$ in the Au/SiO_2/nSi Schottky diode should be 20 meV higher than in Au/PEDOT:PSS/n-Si sample in order to provide the observed widening of the admittance peak. So, the comparison of the two samples shows that the structure

with PEDOT:PSS provides a lower interface state density and lower potential fluctuations as compared to the Au/SiO_2/n-Si structure.

3.3. UPS and XPS measurements. For PEDOT:PSS thin films, the work function, Φ_P, and the position of the valence band edge, E_v, relative to the Fermi level, E_F, were determined by ultraviolet photoemission spectroscopy (UPS) (Figure 6). The work function was calculated from the difference between the excitation energy 21.2 eV and the binding energy at the secondary electron cut-off. For the PEDOT:PSS films a value of Φ_P = (4.8 ± 0.1) eV was found. The position of the valence band edge relative to the Fermi level, E_F-E_v= (0.07±0.02) eV, was obtained by a linear extrapolation of the leading edge of the density of valence band states to zero.

From X-ray photoemission spectroscopy on the Sulphur 2p core-levels the PEDOT/PSS ratio in the film can be calculated, which is one of the factors determining the conductivity of the PEDOT:PSS blend. The S2p XPS spectrum of the PEDOT:PSS thin film is shown on Figure 7. The spectrum is fitted with three components/doublets ($S2p_{1/2}$ and $S2p_{3/2}$ spin-orbit splitting states) corresponding, according to previous studies,[34] to Sulphur atoms in PEDOT (binding energy $S2p_{3/2}$=163.6 eV, asymmetrical component), PSS coordinated to PEDOT or Na (167.5 eV, symmetrical), and PSS coordinated to H (168.2 eV, symmetrical). The PEDOT/PSS molecular ratio obtained from the XPS spectra, 30/70 (±5 %), gives an estimation of the relative surface composition of the PEDOT:PSS film. The determined ratio is consistent with reported ones for SCs with improved conductivity of PEDOT:PSS and enhanced PCE due to optimization of the PSS content by adding different amounts of co-solvents into PEDOT:PSS.[10]

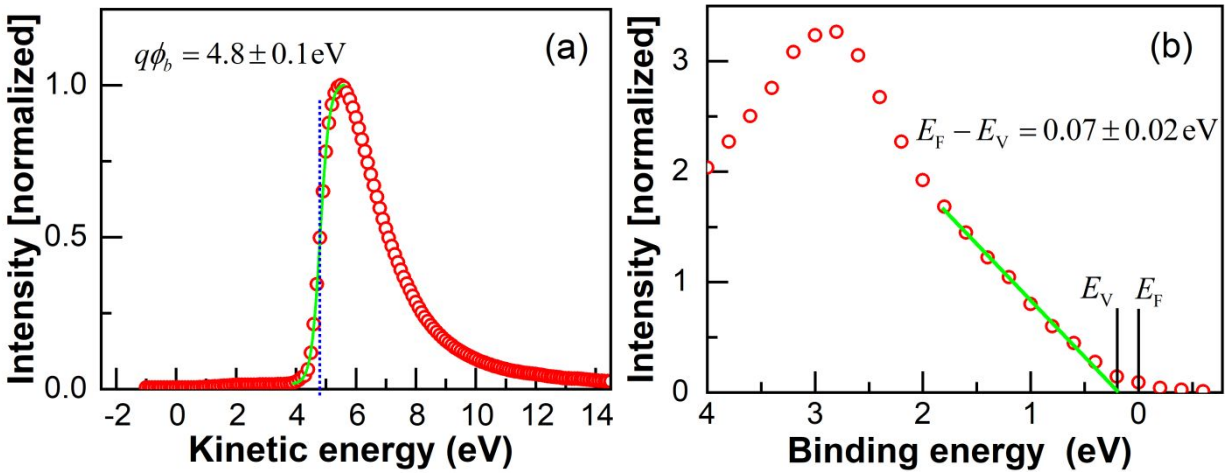

Figure 6. (a) Secondary electron cut-off (SECO) fitted by a Boltzmann sigmoid function for extraction of the work function; (b) Valence band states near the Fermi level E_F with a linear extrapolation to the valence band edge E_V.

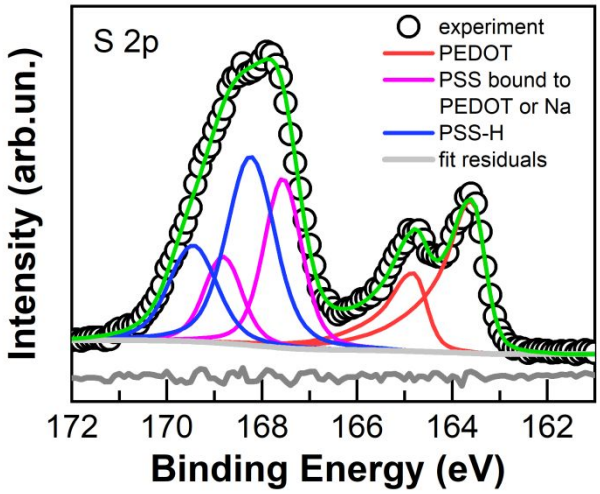

Figure 7. TypicalS 2p XPS spectrum of the PEDOT:PSS film obtained by adding 5% vol% DMSO and 0.025 vol% sodium dodecyl sulfate.

4. Discussion

The value of the built-in potential together with the positions determined of the valence band edge and Fermi level were used to construct a band diagram for the PEDOT:PSS/n-Si junction (Fig.8a). The value of ϕ_B reflects the upward band bending near the Si surface of about 615 meV. Due to the high level of surface passivation of Si wafers by PEDOT:PSS [35] and low

density of the interface traps, the height of the barrier mainly depends on the difference in Fermi level position of the PEDOT:PSS thin films (4.8 eV) and the n-Si substrate (4.3 eV). The work function of the silicon substrate was estimated using standard equation based on the known concentration and ionization energy of phosphorus dopants. The difference between the work function of PEDOT:PSS and silicon (0.5 eV) is smaller than the value derived from C-V measurements (0.615 eV). Taking into account a systematic error of UPS measurements of ±0.1 eV, the observed mismatch can be explained by the presence of the Au top electrode with slightly higher work function of 4.9 eV [36] or 5.1 eV [5].

The barrier height, determined from C-V measurements, exceeds a critical value $\phi_B > |E_F - E_i|$ = 0.24 eV, where E_F is the Fermi energy in Si with a doping concentration of 9.9×10^{14} cm^{-3} and E_i is the middle of the band gap. Therefore, the presence of an inversion layer near the silicon surface should be taken into account for further analysis of the dc transport and admittance characteristics. On the other hand, despite the close values of the work functions of Au and PEDOT:PSS, the Au/SiO_2/n-Si junction does not show an inversion layer due to the formation of interface defects after the deposition of Au on the SiO_2 film. As a result, we observed a depletion layer originating from Fermi level pinning, which limits the potential barrier height near 300 meV (Fig.8b). It is noteworthy that the Au/PEDOT:PSS/SiO_2/n-Si structure without junction between Au and SiO_2, has a potential barrier of 615 meV height as well as an inversion layer near the silicon surface. The reason is that PEDOT:PSS films prevent the formation of Au/SiO_2 interface defects that deteriorate the transport properties of diodes due to enhanced recombination.

In general, Schottky diode or p-n junction models may be applied for the description of the current-voltage, capacitance-voltage, as well as admittance characteristics of PEDOT:PSS/n-Si

junctions. Subject to the validity of the Schottky model, electrons in the semiconductor (majority carriers in Si), which pass over the potential barrier by means of thermionic emission, provide the main contribution to the current at forward biases. [37] However, this possibility is negligibly small due to the electron blocking properties of PEDOT:PSS. As a consequence, the PEDOT:PSS/silicon structure cannot be considered as typical metal-semiconductor Schottky junction, where the polymer film serves as a semitransparent electrode leading to a built-in voltage in the n-type Si wafer.

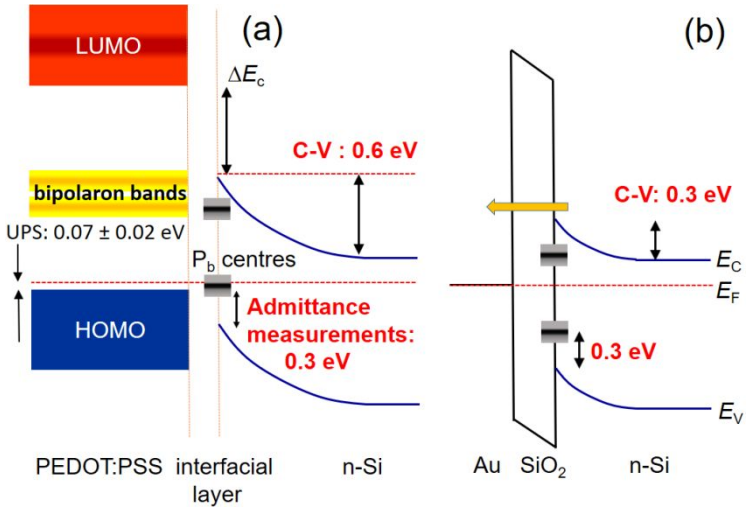

Figure 8. Energy band diagram of the PEDOT:PSS/n-Si junction (a) and the Au/SiO_2/n-Si diode (b).

As follows from the results obtained, the presence of the interfacial defects and an inversion layer near the silicon surface, *i.e.* a p-n junction created inside the semiconductor should be considered. The interface recombination rate is expected to be minimal due to the low electron concentration as compared with holes in the near-surface region of silicon. Further junction improvement requires higher potential barriers, which can be achieved mainly by modifying the work function of nSi or PEDOT:PSS.[38] From this point of view, the role of interface states is not

so critically important for diodes working in the inversion regime if the density of interface states is lower than 10^{13} cm^{-2}.[39] However, despite inversion in the near-surface region of the silicon substrate, the interface states play an important role in the charge carrier transport, trapping, and recombination in PEDOT:PSS/n-Si heterojunctions over a wide temperature range.

An additional complicating factor is the electron blocking property due to the high conduction band offset (see Fig.8a). In order to contribute to the diffusion current at forward bias electrons in Si should overcome the complete potential barrier $\phi_B + \Delta E_C$, which consists of the built-in potential ϕ_B and the conduction band offset ΔE_C. Since thermionic emission of electrons from Si into PEDOT has low probability, the LUMO states don't contribute significantly to conduction. However, electrons have a chance to overcome a lower potential barrier in the space-charge region of Si thus contributing to the forward current. Carrier exchange is possible in the case of alignment of the conduction band of Si with upper states of PEDOT bipolaron bands, the distances of which from the HOMO band are near 0.98 eV and 1.14 eV, correspondingly [36] (see Figure 8). The present mechanism is confirmed by the observation of an Arrhenius behavior of the saturation current J_{01} with an activation energy, which matches well with the built-in potential ϕ_B.

If there were no other transport channels, the forward current would be significantly lower than the experimental values. As follow from the analysis of the J-V dependences measured at different temperatures, one of the main contributions to the forward current is recombination via the PEDOT:PSS/nSi interface states leading to a domination of the term with n=2 in Eq.(1). This is due to the fact that holes in the HOMO band of PEDOT:PSS have a chance to overcome a potential barrier ΔE_V and recombine with electrons in the space-charge region of Si or/and via interface traps. By analyzing the admittance and direct current measurements we can conclude

that the recombination of electrons with holes via interface states associated with a trivalent dangling bond state, so-called P_b centers, at the SiO_2/Si interface has a strong impact on the forward current. To clarify the role of P_b centers we analyzed the temperature dependence of the recombination current, J_{02}. The activation energy of (290±10) meV, determined from an Arrhenius plot of $\ln J_{02}(T)$ vs $1/kT$ for the PEDOT:PSS/n-Si junction, gives an energy distance between the top of the HOMO band and the top of the valence band of Si substrate, *i.e.* potential barriers for holes, which flow from PEDOT:PSS to silicon at the forward bias. In addition, UPS measurements detected the position of Fermi level in the PEDOT:PSS near E_F-E_v= (0.07 ± 0.02) eV (see Figure 8). Therefore, we can conclude that the peak at E_v+0.3 eV of P_b centers is aligned with the Fermi level position, which makes an effective exchange by holes between SiO_x/Si interface states and the HOMO band possible and, therefore, facilitates the recombination process.

Assuming that electrons in Si that pass over the built-in potential would recombine with holes at the PEDOT:PSS/n-Si interface, we can estimate the recombination velocity v_I from Equation (1), where $J_{02} = qD_{it}v_I$ is the dark recombination current, D_{it} is the density of interface traps derived from admittance spectroscopy. This leads to an interface recombination velocity of 480 cm/s at 295 K for the PEDOT:PSS/n-Si junction. Such a low surface recombination rate is due to a reduced concentration of electrons (majority carriers) near the silicon surface in the inversion regime preventing their recombination with holes via interface states.

The estimated recombination velocity fits well to the observation for the SiO_2/Si interface, which is usually in the order of 1000 cm/s.[40] This means that the forward current in Au/PEDOT:PSS/n-Si structures is determined by the recombination efficiency through the states associated with SiO_x/Si interface traps, namely P_b centers. Due to microvoids in the PEDOT:

PSS films, this interface is non-uniform, because both the PEDOT:PSS/n-Si and SiO_x/n-Si junctions are present. As it was concluded in [7], it is impossible to avoid the formation of an ultrathin SiO_x layer on the Si surface while producing PEDOT:PSS/n-Si heterojunctions due to the short contact with ambient atmosphere after removing from the HF acid, oxygen diffusion through PEDOT:PSS thin film, and oxidation of the Si surface by PSS species.[35] The presence of 1.6 nm thick SiO_x films on the Si surface was detected by spectroscopic ellipsometry measurements in the studied PEDOT:PSS/n-Si junctions (see Figure S3 in the Supporting information). Thus, despite the production of polymer films immediately after HF treatment, it was not possible to avoid the formation of an oxide layer, the presence of which could greatly affect the transport properties of solar cells.[41] In addition to the expected improvement of carrier separation due to inducing band bending in the Si substrate, the interfacial oxide increases the serial resistance and limits the current. As a consequence, the temperature dependence of the serial resistance demonstrates an activation behavior with an energy of (290±10) meV, which agrees well with the position of hole traps at E_v+0.3eV.

Thus, these results suggest that the electrical transport mechanisms of the PEDOT:PSS/Si heterojunction are determined by interfacial defects associated with P_b centers with deep levels in the silicon band gap.

Conclusions

In conclusion, we addressed the origin of interface states of conducting polymer PEDOT:PSS on n-type silicon wafers. The charge transport mechanism in the hybrid solar cells was experimentally studied using admittance spectroscopy, current-voltage and capacitance-voltage measurements. The potential barrier height of diodes was found to be determined mainly by the difference in work function of the PEDOT:PSS and Si indicating a low density of interface

states. In order to describe the J-V dependences measured at different temperatures we consider two models for the system. The first one is a typical metal-semiconductor Schottky junction based on thermionic emission of majority carriers, electrons in n-Si, over a built-in potential barrier in the near-surface region. Assuming that the PEDOT:PSS polymer film serves as a semitransparent electrode with a work function close to Au, it is not able to explain the behavior of the forward branch of the J-V dependences of PEDOT:PSS/n-Si and PEDOT:PSS/SiO_2/n-Si structures measured at low temperatures in comparison with the data for the Au/SiO_2/n-Si diodes.

The key to understand the origin of charge carrier transport in the PEDOT:PSS/n-Si solar cells is that the samples studied show a strong inversion near the silicon surface, *i.e.* the presence of a p-n junction inside the semiconductor leading to the low recombination losses. The interface recombination rate was found to be around 480 cm/s at 295 K, while the interface state density was equal to 2.5×10^{10} $cm^{-2}eV^{-1}$ for Au/PEDOT:PSS/n-Si. The second, two diode model including parallel and serial resistance was applied for the numerical analysis of the J-V curves measured at different temperatures. We show that the observed dependences can be understood within the inversion layer model in terms of the diffusion of minority carriers in silicon, blocking of electron flow at forward biases, as well as dominating recombination current associated with P_b centers at the PEDOT:PSS/n-Si interface.

Associated content

Supporting Information.

The Supporting Information is available free of charge on the ACS Publications website at DOI; AFM images of PEDOT:PSS film on silicon surface, J-V characteristics under AM1.5 spectrum irradiation of the hybrid PEDOT:PSS/n-Si solar cell, and spectral ellipsometry data.

Author information

Corresponding Author

* kondr@univ.kiev.ua

Acknowledgment

S.V. Kondratenko is grateful to DAAD (Funding programme ID 57314018, Personal ref. No. 91653170) for the scholarship supporting his research stay at Chemnitz University of Technology.

References

(1) Hwang, J.; Amy, F.; Kahn A. Spectroscopic study on sputtered PEDOT PSS: Role of surface PSS layer. *Org. Electron.* **2006**, *7*, 387-396.

(2) Schmidt, J.; Titova, V.; Zielke, D. Organic-silicon heterojunction solar cells: Open-circuit voltage potential and stability. *Appl. Phys. Lett*. **2013**, *103*(18), 183901.

(3) Kirchmeyer, S.; Reuter, K. Scientific importance, properties and growing applications of poly(3,4-ethylenedioxythiophene). *J. Mater. Chem*. **2005**,*15*, 2077-2088.

(4) Jäckle, S.; Liebhaber, M.; Gersmann, C.; Mews, M.; Jäger K.; Christiansen, S.; Lips, K. Potential of PEDOT:PSS as a hole selective front contact for silicon heterojunction solar cells. *Sci. Rep.* **2017**, *7*, 2170.

(5) Jäckle, S.; Mattiza, M.; Liebhaber, M.; Brönstrup, G.; Rommel, M.; Lips, K.; Christiansen, S. Junction Formation and Current Transport Mechanisms in Hybrid n-Si/PEDOT:PSS Solar Cells. *Sci. Rep.* **2015**, *5*, 13008.

(6) Price, M. J.; Foley, J. M.; May, R. A.; and Maldonado, S. Comparison of Majority Carrier Charge Transfer Velocities at Si/Polymer and Si/Metal Photovoltaic Heterojunctions. *Appl. Phys. Lett.*, **2010**, *97*, 083503.

(7) Zhang, C.; Zhang, Y.; Guo, H.; Jiang, Q.; Dong, P.; Zhang, C. Efficient Planar Hybrid n-Si/PEDOT:PSS Solar Cells with Power Conversion Efficiency up to 13.31% Achieved by Controlling the SiO_x Interlayer, *Energies* **2018**, *11*, 1397.

(8) Zhang, F.; Liu, D.; Zhang, Y.; Wei, H.; Song, T.; Sun. B. Methyl/Allyl Monolayer on Silicon: Efficient Surface Passivation for Silicon-Conjugated Polymer Hybrid Solar Cell. *ACS Appl. Mater. Interfaces* **2013**, *5*(11), 4678-4684.

(9) Thomas, J. P.; Zhao, L.; McGillivray, D.; Leung, K. T. High-Efficiency Hybrid Solar Cells by Nanostructural Modification in PEDOT:PSS with Co-solvent Addition. *J. Mater. Chem. A* **2014**, *2*, 2383-2389.

(10) Thomas, J. P.; Leung, K. T., Defect-Minimized PEDOT:PSS/Planar-Si Solar Cell with Very High Efficiency. *Adv. Funct. Mater*. **2014**, *24*, 4978-4985.

(11) Khatri, I.; Imamura, T.; Uehara, A.; Ishikawa, R.; Ueno, K.; Shirai, H.Chemical mist deposition of graphene oxide and PEDOT:PSS films for crystalline Si/organic heterojunction solar cells, *Phys. Status Solidi C* **2012**, *9*, 2134.

(12) Jiang, Y.; Gong, X.; Qin, R.; Liu, H.; Xia, C.; Ma, H., Efficiency Enhancement Mechanism for Poly(3, 4-ethylenedioxythiophene): Poly(styrenesulfonate)/Silicon Nanowires Hybrid Solar Cells Using Alkali Treatment. *Nanoscale Res Lett* **2016**, *11*, 267.

(13) Zhang, Y.; Liu, R.; Lee, S.-T.; Sun, B. The role of a LiF layer on the performance of poly(3,4-ethylenedioxythiophene): poly(styrenesulfonate)/Si organic-inorganic hybrid solar cells. *Appl. Phys. Lett*. **2014**, *104*, 083514.

(14) Shockley, W.; Queisser, H.J. Detailed balance limit of efficiency of p–n junction solar cells. *J. Appl. Phys*. **1961**, *32*, 510.

(15) Zhu, J.; Yang, Xi; Sheng, J.; Gao, P.; Ye., J. Double-Layered PEDOT:PSS Films Inducing Strong Inversion Layers in Organic/Silicon Hybrid Heterojunction Solar Cells. *ACS Appl. Energy Mater.* **2018**, *1*(6), 2874-2881.

(16) Nagamatsu, K.; Avasthi, S.; Jhaveri, J.; Sturm J. A 12% Efficient Silicon/PEDOT:PSS Heterojunction Solar Cell Fabricated at < 100 °C. *IEEE Journal of Photovoltaics*. **2014**, *4*(1), 260-264.

(17) Yang, Z; Gao, P.; He, J.; Chen, W.; Yin, W.-Y.; Zeng, Y.; Guo, W.; Ye, J.; Cui, Y. Tuning of the Contact Properties for High-Efficiency Si/PEDOT:PSS Heterojunction Solar Cells. *ACS Energy Lett.* **2017**, *2*, 556−562.

(18) Sheng, J.; Fan, K.; Wang, D.; Han, C.; Fang, J.; Gao, P.; Ye, J. Improvement of the SiOx Passivation Layer for High-Efficiency Si/ PEDOT:PSS Heterojunction Solar Cells. *ACS Appl. Mater. Interfaces* **2014**, *6*, 16027−16034.

(19) Sze, S. M.; Ng, K. K. Physics of Semiconductor Devices. (Wiley, 2006).

(20) Suckow, S. 2/3-Diode Fit, [Online], 2014. Available: ⟨http://nanohub.org/ resources/14300⟩.

(21) Green, M. Recent developments in photovoltaics. *Sol. Energy* **2004**, *76*, 3−8.

(22) Losee, D.L. Admittance spectroscopy of impurity levels in Schottky barriers. *J. Appl. Phys.* **1975**, *46*, 2204–2214.

(23). Oldham, W. G.; Naik, S. S. Admittance of p-n junctions containing traps. *Solid-State Electronics* **1972**, 15, 1085–1086.

(24) Derdouri, M.; Mahdjoubi, L.; Benmalek, M. Analysis of admittance spectroscopy method for the study of deep levels. *Solid-State Electronics* **1982**, *25*, 925–931.

(25) Walter, T.; Herberholz, R.; Müller, C.; Schock, H. W. Determination of defect distributions from admittance measurements and application to Cu(In,Ga)Se2 based heterojunctions. *Journ. Appl. Phys.* **1996**, *80*, 4411-4420.

(26) Vincent, G.; Bois, D.; Pinard, P. Conductance and capacitance studies in GaP Schottky barriers. *Journ. Appl. Phys*. **1975**, *46*, 5173-5178.

(27) Casey, H. C., Jr.; Cho, A. Y.; Lang, D. V.; Nicollian, E. H. Measurement of MIS capacitors with oxygen-doped AlxGa1-xAs insulating layers on GaAs. *Journ. Vac. Sci. and Technol*. **1978**, *15*, 1408–1411.

(28) Barret, C.; Chekir F.; Vapaile, A. Study of metal-semiconductor interface states using Schottky capacitance spectroscopy. *J. Phys. C: Solid State Phys.* **1983**, *16*, 2421-2438.

(29) Altındal, Ş.; Yücedağ, İ.; Tataroğlu, A. Analysis of surface states and series resistance in Au/n-Si Schottky diodes with insulator layer using current–voltage and admittance–voltage characteristics. *Vacuum* **2009**, *84*, 363–368.

(30) Khelifi, S.; Decock, K.; Lauwaert, J.; Vrielinck, H.; Spoltore, D.; Piersimoni, F.; Manca, J.; Belghachi, A.; Burgelman, M. Investigation of defects by admittance spectroscopy measurements in poly (3-hexylthiophene):(6,6)-phenyl C61-butyric acid methyl ester organic solar cells degraded under air exposure. *Journ. Appl. Phys*. **2011**, *110*, 094509.

(31) Nicollian, E. H.; Bruce, J. R. MOS Physics and Technology (Wiley, New York 1982).

(32) Caplan, P. J.; Poindexter, E. H.; Deal, B. E.; Razouk, R. R. ESR centers, interface states, and oxide fixed charge in thermally oxidized silicon wafers.*J. Appl.Phys*. **1979**, *50*, 5847.·

(33) Gomeniuk, Y. Y.; Gomeniuk, Y. V.; Nazarov, A. N.; Lysenko, V. S.; Osten, H. J.; Laha, A. Interface and Bulk Properties of High-K Gadolinium and Neodymium Oxides on Silicon. *Advanced Materials Research* **2011**, *276*, 167-178.

(34) G. Zotti, S. Zecchin, G. Schiavon, F. Louwet, L. Groenendaal, X. Crispin, W. Osikowicz, and W. Salaneck, M. Fahlman, Electrochemical and XPS Studies toward the Role of Monomeric

and Polymeric Sulfonate Counterions in the Synthesis, Composition, and Properties of Poly(3,4-ethylenedioxythiophene) *Macromolecules* **2003**, *36*, 3337-3344.

(35) Chen, J.; Shen, Y.; Guo, J.; Chen, B.; Fan, J.; Li, F.; Liu, B.; Liu, H.; Xu, Y.; Mai, Y. Electrochemical grafting passivation of silicon via electron transfer at polymer/silicon hybrid interface. *Electrochimica Acta* **2017**, *247*, 826–834.

(36) Demtchenko, S.; Tarr, N. G.; McGarry, S. Effect of PEDOT band structure on conductive polymer-insulator-silicon junctions. *Journ. Appl. Phys.* **2017**, *122*, 065502.

(37) Zhu, Y.; Song, T.; Zhang, F.; Lee, S.-T.; Sun, B. Efficient organic-inorganic hybrid Schottky solar cell: The role of built-in potential. *Appl. Phys. Lett*. **2013**, *102*, 113504.

(38) Shen, X.; Chen, L.; Pan, J.; Hu, Y.; Li, S.; Zhao, J. Improved Work Function of Poly(3,4-ethylenedioxythiophene): Poly(styrenesulfonic acid) and its Effect on Hybrid Silicon/Organic Heterojunction Solar Cells *Nanoscale Research Letters* **2016**, *11*, 532.

(39) Bardeen, J. Surface States and Rectification at a Metal Semi-Conductor Contacts. *Phys. Rev.* **1947**, *71*, 717-727.

(40) Mäckel, H.; Cuevas, A. Determination of the surface recombination velocity of unpassivated silicon from spectral photoconductance measurements. *Proc. 3rd World Conf. Photovolt. Energy Convers.* **2003**, *1*, 71 – 74.

(41) He, L.; Jiang, C.; Wang, H.; Lai, D.; Rusli, High efficiency planar Si/organic heterojunction hybrid solar cells. *Appl. Phys. Lett*. **2012**, *100*, 073503.

Table of Contents Graphic